



Cite this: DOI: 10.1039/c9tb00946a

A reversible, switchable pH-driven quaternary ammonium pillar[5]arene nanogate for mesoporous silica nanoparticles†

Evelyn C. S. Santos,^{id a} Thiago C. dos Santos,^{id a} Tamires S. Fernandes,^{id a} Fernanda L. Jorge,^{id c} Vanessa Nascimento,^{id d} Vinicius G. C. Madriaga,^{id a} Pâmella S. Cordeiro,^{id d} Noemi R. Checca,^{id b} Nathalia Meireles Da Costa,^{id c} Luis Felipe Ribeiro Pinto^{id c} and Célia M. Ronconi^{id *a}

Here we describe the assembly and pH-driven operation of two nanocarriers based on non-functionalized (MCM-41) and carboxylate-functionalized (MCM-41-COOH) containers loaded with the anticancer drug doxorubicin (DOX) and capped by quaternary ammonium pillar[5]arene (P[5]A) nanogates. MCM-41 and MCM-41-COOH containers were synthesized and transmission and scanning electron microscopies showed nanoparticles with spherical morphology and dimensions of 85 ± 13 nm. The nanochannels of MCM-41 loaded with DOX were gated through the electrostatic interactions between P[5]A and the silanolate groups formed at the silica–water interface, yielding the MCM-41-DOX-P[5]A nanocarrier. The second nanocarrier was gated through the electrostatic interactions between the carboxylate groups mounted on the surface of MCM-41 and P[5]A, resulting in the MCM-41-COO-DOX-P[5]A nanocarrier. The DOX release profiles from both nanocarriers were investigated by UV-vis spectroscopy at different pH values (2.0, 5.5 and 7.4) and also in the presence of ions, such as citrate³⁻ (19 mmol L⁻¹) and Zn²⁺ (1.2 and 50 mmol L⁻¹) at 37 °C. MCM-41-COO-DOX-P[5]A can be turned on and off eight times through the formation and breaking of electrostatic interactions. *In vitro* studies show that MCM-41-COO-DOX-P[5]A can penetrate and release DOX in the nucleus of human breast adenocarcinoma MCF-7 cancer cells leading to a pronounced cytotoxic effect. Therefore, the fabricated nanocarrier based on a water-soluble cationic pillar[5]arene nanogate, which is reversibly opened and closed by electrostatic interactions, can be considered as a promising drug transport and delivery technique for future cancer therapy.

Received 10th May 2019,
Accepted 6th December 2019

DOI: 10.1039/c9tb00946a

rsc.li/materials-b

Introduction

The use of gated nanocarriers for the smart controlled release of chemotherapy drugs has attracted considerable attention as a potential alternative system for cancer treatment.^{1–3} These systems can be built by attaching supramolecular binding stations on mesoporous silica nanoparticles (MSNPs) to interact with moving

components, which reversibly open and close the nanochannel entryways of the MSNPs to allow content release by an external stimulus,^{4–9} such as light/heat irradiation,^{10–12} a pH change,^{4,13,14} alternating magnetic field application,¹⁵ and enzymatic¹⁶ and redox reactions.^{17,18}

Various macrocycles can be used as moving components or nanogates to seal the nanochannels and prevent content leakage, e.g., cyclodextrins,¹⁸ crown ethers,¹⁹ cucurbiturils² and calixarenes.²⁰ Pillar[n]arenes are emerging as a novel class of synthetic macrocycle paracyclophane derivatives that consist of 1,4-disubstituted hydroquinone units linked by methylene bridges in their *para*-positions. They have an electron-rich cavity and high symmetry and can be chemically modified at both the upper and lower rims in contrast to other macrocycles.^{21–26} The first water-soluble pillar[5]arene was synthesized in 2010 by introducing carboxylate groups around the rims of a macrocycle.²⁷ Water-soluble pillararenes have considerable applications in the field of mechanochemistry.^{28–30} For example, a carboxylic acid-substituted pillar[5]arene (CP[5]) has been used as a moving

^a Departamento de Química Inorgânica, Universidade Federal Fluminense, Campus do Valonguinho, Outeiro São João Batista s/n, Centro, 24020-150, Niterói, RJ, Brazil. E-mail: cmronconi@id.uff.br

^b Centro Brasileiro de Pesquisas Físicas (CBPF), Dr Xavier Sigaud 150, Urca, 22290-180, Rio de Janeiro, RJ, Brazil

^c Molecular Carcinogenesis Program, Instituto Nacional de Câncer (INCA), André Cavalcanti 37, Centro, 20231-050, Rio de Janeiro, RJ, Brazil

^d Departamento de Química Orgânica, Universidade Federal Fluminense, Campus do Valonguinho, Outeiro São João Batista s/n, Centro, 24020-150, Niterói, RJ, Brazil

† Electronic supplementary information (ESI) available. See DOI: 10.1039/c9tb00946a

component in nanovalves.^{4,13,14,31–38} However, the water-soluble quaternary ammonium pillar[5]arene (P[5]A) has not been extensively explored, and to the best of our knowledge, it has not been reported in the literature as a nanogate. Cationic P[5]A has the advantage of interacting electrostatically with the negatively charged surface of MSNPs through the conjugate base silanolate that forms at the silica–water interface; thus, functionalization may not be required, eliminating one step in the assembly of the nanodevice.

In this work, we explored the use of the water-soluble quaternary ammonium pillar[5]arene P[5]A, as a nanogate in the construction of two nanocarriers. P[5]A was employed as a stopper to seal the nanochannels of MSNPs through simple electrostatic interactions between the positively charged ammonium groups located on the upper and lower rims of P[5]A and the negatively charged surface of the MSNPs. We assembled the first nanocarrier by mounting the P[5]A nanogate directly on non-functionalized MCM-41 (MCM-41-DOX-P[5]A) and the second one by mounting P[5]A on carboxylate group-functionalized MCM-41 (MCM-41-COO-DOX-P[5]A). The nanocarriers were loaded with doxorubicin (DOX), and the release of the drug was investigated (Scheme 1). P[5]A was found to strongly interact with the silanolate groups of non-functionalized MCM-41 and not fully disconnect on command (acid pH). In contrast, P[5]A coupled to carboxylate group-functionalized MCM-41 (MCM-41-COO-DOX-P[5]A) not only obeys commands but also can be reversibly switched eight times in response to pH changes.

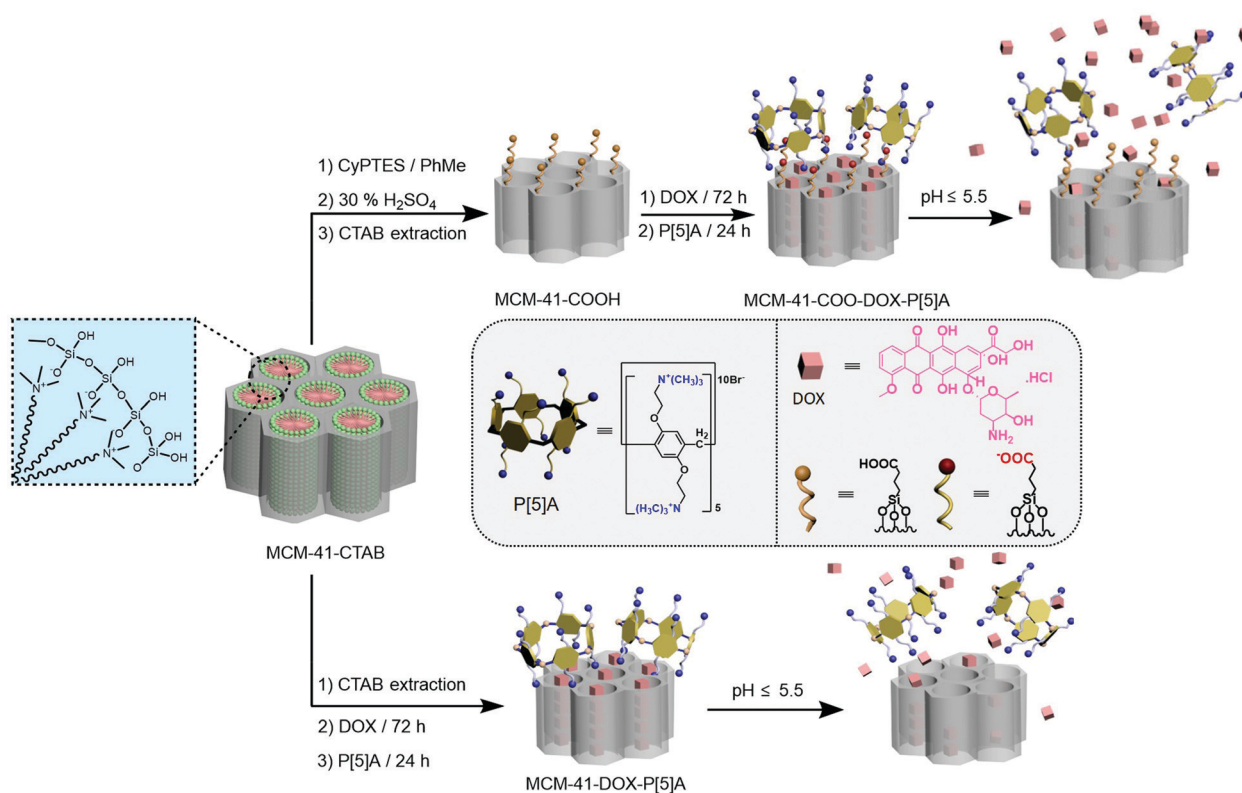
The capacity of MCM-41-COO-DOX-P[5]A to deliver doxorubicin inside human breast adenocarcinoma MCF-7 cancer cells was also evaluated.

Results and discussion

Synthesis and characterization of P[5]A, MCM-41, MCM-41-CN and MCM-41-COOH

The cationic pillar[5]arene was synthesized using the general procedure introduced by Ogoshi.^{22,39} Typically, hydroquinone bis(2-hydroxyethyl)ether was converted to the brominated hydroquinone **1** by the Appel reaction. Then, the cyclization of compound **1** with paraformaldehyde was carried out in the presence of the Lewis acid $\text{BF}_3 \cdot \text{OEt}_2$ and the template dichloromethane to yield brominated pillar[5]arene **2**. Compound **2** was converted to the quaternary ammonium pillar[5]arene named P[5]A by reacting with trimethylamine in ethanol (Scheme S1, ESI[†]).³⁹ The product P[5]A was characterized by ^1H and ^{13}C NMR spectroscopy (Fig. S1 and S2, ESI[†]).

MCM-41 was synthesized by a base-catalyzed sol-gel method using a cationic surfactant (hexadecyltrimethylammonium bromide, CTAB) template following the procedures described by Zink *et al.*^{40–42} To functionalize MCM-41 with carboxyl groups we used a methodology employed by our group to modify silica nanoparticles with various functional groups.^{17,18,43–50} MCM-41 containing the CTAB template (MCM-41-CTAB) in the pores was



Scheme 1 Schematic representation of the preparation of DOX-loaded MCM-41-COO[−] and its interaction with the positively charged P[5]A nanogate. The same procedure was carried out for non-functionalized MCM-41. MCM-41-COO-DOX-P[5]A and MCM-41-DOX-P[5]A can be operated by chemical stimulus (pH changes) to regulate the release of doxorubicin (DOX).

modified with 3-cyanopropyltriethoxysilane (CyPTES) to form MCM-41-CTAB-CN, followed by the acid-catalyzed hydrolysis of the 3-cyanopropyl groups to produce 3-carboxypropyl groups on the surface of the MCM-41. CTAB template extraction from the pores was carried out using ethanolic ammonium chloride to form the compound named MCM-41-COOH.

The FTIR spectra of MCM-41-CTAB, MCM-41, MCM-41-CN, and MCM-41-COOH show bands at 1060 and 803 cm^{-1} , which are ascribed to the asymmetric and symmetric stretching of Si–O–Si bonds, respectively (Fig. S3, ESI†). The band at 947 cm^{-1} is due to the Si–OH stretching mode.⁵¹ The bands at 2926 and 2852 cm^{-1} and the band in the region of 1400–1500 cm^{-1} of the spectrum of MCM-41-CTAB are assigned to the C–H stretching and C–H bending vibration modes of methyl and methylene groups of CTAB.⁵² The absence of the bands related to CTAB in both the MCM-41-CN and MCM-41-COOH materials indicates that the template was successfully removed. The Raman spectrum of MCM-41-CN shows a weak band at 2249 cm^{-1} due to the C≡N stretching vibration mode (Fig. S4, ESI†).^{53,54} The band at 1717 cm^{-1} in the FTIR spectrum for MCM-41-COOH is due to the C=O stretching vibration mode, confirming the oxidation of 3-cyanopropyl groups into 3-carboxypropyl groups.⁵⁵ The oxidation of the cyano groups was also confirmed by elemental analysis, which showed carbon and nitrogen contents of 8.3 and 1.9 mmol g^{-1} , respectively, for MCM-41-CN. After the hydrolysis of the cyano groups, the carbon content reduced to 5.8 mmol g^{-1} and 0.3 mmol g^{-1} of nitrogen was detected in the MCM-41-COOH sample. Most likely, the reduction in the carbon content is related to the possible leaching of organosilane chains from the surface of MCM-41-COOH during the hydrolysis step.

The nitrogen adsorption–desorption isotherms of MCM-41 are type IV(b), indicating the presence of cylindrical mesopores with a diameter smaller than 4 nm.^{56,57} This material exhibits a surface area of 1034 $\text{m}^2 \text{g}^{-1}$, a pore volume of 1.14 $\text{cm}^3 \text{g}^{-1}$ and a narrow pore distribution of 2.72 nm based on the Barrett–Joyner–Halenda (BJH) method (Fig. S5, S6 and Table S1, ESI†). PXRD analysis of MCM-41 shows three reflection angles at $2\theta = 2.15, 3.71$ and 4.30 , indexed as (100), (110) and (200) Bragg peaks, respectively (Fig. S7, ESI†). The (100) reflection is associated with the hexagonal structure of MCM-41, and the other reflections are due to the crystallinity.⁵⁸ Scanning electron microscopy (SEM) of MCM-41 shows spherical particles with a size distribution centered at $85 \text{ nm} \pm 13 \text{ nm}$ (Fig. S8, ESI†). Transmission electron microscopy (TEM) shows a well-ordered hexagonal mesoporous structure of MCM-41 (Fig. S8, ESI†).

Upon functionalization of MCM-41 with carboxyl groups (MCM-41-COOH), the nitrogen adsorption–desorption isotherms remain of type IV(b), thus the mesoporous structure was not damaged (Fig. S5, ESI†); however, the surface area, pore volume and pore diameter decreased to 755 $\text{m}^2 \text{g}^{-1}$, 0.97 and 2.54 nm, respectively (Table S1, ESI†). The PXRD pattern of MCM-41-COOH shows a decrease in all peak intensities, suggesting a crystallinity reduction (Fig. S7, ESI†). The TEM images clearly show that the well-ordered hexagonal mesoporous structure remains after the acid hydrolysis process (Fig. S9, ESI†). The diameters of MCM-41 and MCM-41-COOH measured by dynamic light

scattering (DLS) are 170.3 and 211.9 nm, respectively, indicating that both materials are well dispersed in aqueous medium (Fig. S10, ESI†).

The zeta potential (ζ -potential) values of MCM-41 and MCM-41-COOH are -14.8 and -30.2 mV at pH = 7.4, respectively (Fig. S11, ESI†). The ζ -potential values of both MCM-41 and MCM-41-COOH become more negative with increasing pH due to the deprotonation of the silanol and carboxypropyl groups, respectively. MCM-41-COOH shows more negative ζ -potential values than MCM-41 because the carboxypropyl groups are more acidic than the silanol groups; therefore, more deprotonated species form on its surface.

To confirm the higher acidity of MCM-41-COOH compared to that of MCM-41, potentiometric titrations were carried out (Fig. S12, ESI†). The Gran plots (Fig. S13, ESI†) show that the pK_a and the concentration of the acid sites are 7.2 and 154 $\mu\text{mol g}^{-1}$ for MCM-41 and 6.1 and 582 $\mu\text{mol g}^{-1}$ for MCM-41-COOH (Table S2, ESI†).^{59,60} Therefore, functionalization with carboxypropyl groups improved the acidity of MCM-41, as expected.

FTIR spectroscopy of DOX-unloaded MCM-41-P[5]A and MCM-41-COO-P[5]A

Before loading the nanochannels of the MSNPs with DOX, the electrostatic interactions between the cationic pillar[5]arene P[5]A and MCM-41 and MCM-41-COOH were investigated by FTIR spectroscopy (Fig. S14, ESI†). The P[5]A salt shows absorption bands at 1612 cm^{-1} and 1486 cm^{-1} due to the phenyl skeleton stretching vibration C=C, 1204 and 1063 cm^{-1} related to the asymmetric and symmetric stretching vibration of aryl alkyl ether C–O–C.^{61–63} The absorption band at 1717 cm^{-1} , assigned to the C=O stretching vibration of the carboxylic acid group of MCM-41-COOH, disappears in MCM-41-COO-P[5]A due to the formation of carboxylate groups that electrostatically interact with P[5]A. We should expect the absorption bands at 1650 and 1400 cm^{-1} to be related to the asymmetric and symmetric vibration modes, respectively, of $(\text{COO})^-$ in MCM-41-COO-P[5]A; however, these absorption bands may overlap with the quaternary ammonium P[5]A absorption bands.

Colloidal studies on the interaction between cationic P[5]A and MCM-41 and MCM-41-COOH

The interactions between P[5]A and MCM-41 and MCM-41-COOH were also investigated by measuring the zeta potential (ζ -potential) changes of their dispersions in phosphate buffered saline (PBS) solutions containing 0.5 mg mL^{-1} of MCM-41 or MCM-41-COOH as a function of the P[5]A concentration (Fig. 1).

As previously discussed (Fig. S11, ESI†), at pH 7.4, MCM-41 and MCM-41-COOH are negatively charged because silanolate and carboxylate groups form at the interface between the solids and water; both can electrostatically interact with P[5]A. Prior to the addition of P[5]A, the ζ -potential values of MCM-41 and MCM-41-COOH were -14.8 and -30.2 mV, respectively, at pH 7.4 and room temperature (Fig. 1 and S11, ESI†). The isoelectric points (IEPs) of the MCM-41 and MCM-41-COOH dispersions were reached at a concentration of 86.8 mg L^{-1} of P[5]A (Fig. 1).

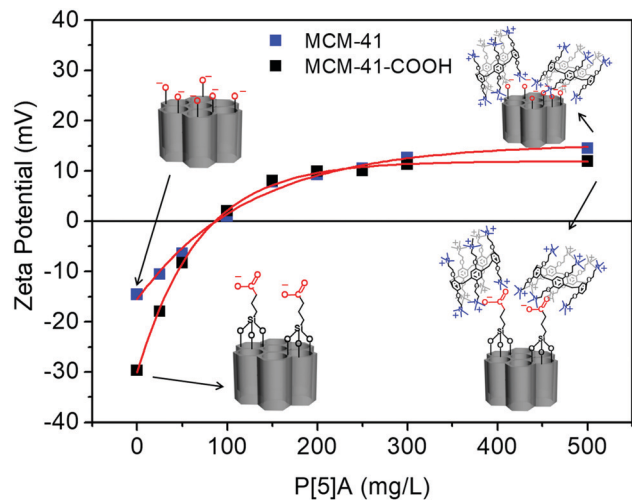


Fig. 1 ζ -Potential measurements as a function of P[5]A concentration for MCM-41 and MCM-41-COOH at pH = 7.4 and RT in PBS buffer.

Higher concentrations of P[5]A shifted the ζ -potential to positive values, and then it became almost constant at concentrations higher than 200 mg L⁻¹ for both materials. The positive values of the ζ -potential are related to the positive P[5]A-silica-water interface (named MCM-41-P[5]A or MCM-41-COO-P[5]A), in which the non-interacting rims of P[5]A provide the surface charge in colloidal suspensions. Additionally, for concentrations above 200 mg mL⁻¹ of P[5]A, the ζ -potential values did not significantly change because the negative surfaces of MCM-41 and MCM-41-COOH were saturated with P[5]A, and the excess of P[5]A did not interact with the MSNP surfaces.

The effects of pH (2.0–12.0) on the interactions between P[5]A and MCM-41 or MCM-41-COOH were also investigated by ζ -potential measurements (Fig. 2). The ζ -potential values of MCM-41 and MCM-41-COOH suspensions in PBS, both capped with P[5]A (MCM-41-P[5]A or MCM-41-COO-P[5]A), are +21.4 and +11.1 mV, respectively, at pH 7.4 as a result of the interactions

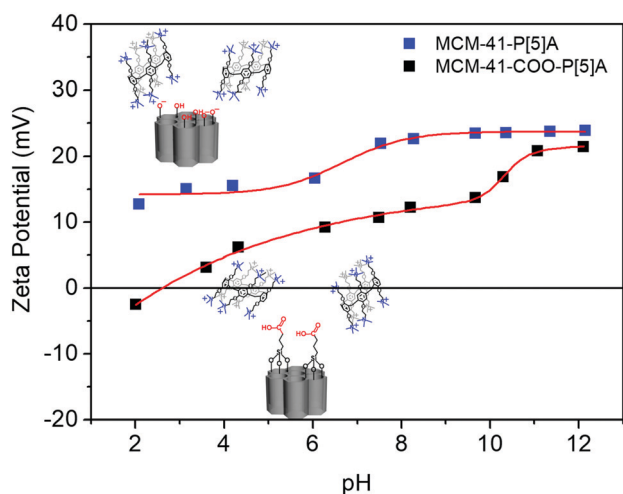


Fig. 2 ζ -Potential measurements as function of pH for MCM-41-P[5]A and MCM-41-COO-P[5]A.

between P[5]A and the surfaces (Fig. 2). The ζ -potential values gradually decrease upon the acidification of the dispersions due to the protonation of the silanolate or carboxylate groups (Fig. 2). The IEP of the MCM-41-COO-P[5]A dispersion is at pH = 2.6. This result demonstrates that at an acidic pH, the protonation of the carboxylate groups in MCM-41-COO-P[5]A occurs because the surface charge shifts to zero, releasing the macrocycle P[5]A into the solution.

For MCM-41-P[5]A, the ζ -potential values are positive over the entire pH range (2.0–12.0), indicating that P[5]A remains on MCM-41 even under very acidic conditions (pH = 2.1). The inner diameter of the paracyclophane moiety of the optimized structure of P[5]A is 0.84 nm, and the distance between the two opposite quaternary ammonium groups located on the same side of the rim is 1.64 nm (Fig. S15, ESI[†]). Therefore, P[5]A can also interact with the silanolate groups located inside the pores of the unloaded MCM-41. Upon the addition of acid, the silanolate groups on the external surface of MCM-41 are easily protonated, and the P[5]A stoppers are released. However, those located inside the empty pores remain.

Characterization of DOX-unloaded and loaded nanocarriers by N₂ adsorption-desorption isotherms

The amounts of DOX loaded in MCM-41-DOX-P[5]A and MCM-41-COO-DOX-P[5]A were obtained from a DOX standard curve monitoring the DOX absorption band at 483 nm (Fig. S16, ESI[†]).^{17,26,64} The calculated amounts of loaded DOX were 27.2 mg g⁻¹ (MCM-41-DOX-P[5]A) and 28.6 mg g⁻¹ (MCM-41-COO-DOX-P[5]A) corresponding to a DOX-loading efficiency of 52.4% and 57.6%, respectively. For the detailed calculations, see the Experimental section.

To investigate the effect of the P[5]A stopper and the drug on the mesopore structure of the MSNPs, the N₂ adsorption-desorption isotherm curves of the DOX-unloaded (MCM-41-P[5]A and MCM-41-COO-P[5]A) and DOX-loaded nanocarriers (MCM-41-DOX-P[5]A and MCM-41-COO-DOX-P[5]A) were measured. The isotherms of MCM-41-P[5]A and MCM-41-COO-P[5]A showed type III profiles, which are characteristic of nonporous materials (Fig. S5 and Table S1, ESI[†]). Condensation and evaporation phenomena in the region of 0.2 bar < p/p^0 < 0.4 bar are absent in these isotherms indicating complete mesopore obstruction due to the presence of the P[5]A stopper. Similar behaviors were observed for the isotherms of DOX-loaded MCM-41-DOX-P[5]A and MCM-41-COO-DOX-P[5]A nanocarriers (Fig. S5, ESI[†]). The BJH pore size distributions confirmed the absence of mesopores in the DOX-unloaded and loaded nanocarriers (Fig. S6, ESI[†]).

pH-Trigged DOX release from MCM-41-DOX-P[5]A and MCM-41-COO-DOX-P[5]A

The efficiency of P[5]A in blocking the nanochannel entryways on MCM-41 and MCM-41-COOH and avoiding drug release at physiological conditions (37 °C and pH 7.4) was evaluated by monitoring the absorption band of DOX at 483 nm over time in the UV-vis spectrum. The amounts of DOX released were calculated from its standard curve (Fig. S16, ESI[†]). The DOX leakage in the capped MCM-41-COO-DOX-P[5]A nanocarrier is

lower (4%) than that observed for MCM-41-DOX-P[5]A (11%) within 30 h. These are minimal and acceptable leakages, as reported in the literature for other systems.^{16,19,65} Therefore, these findings demonstrate that the water-soluble quaternary ammonium pillar[5]arene, P[5]A, can block the nanochannel entryways on MCM-41 and MCM-41-COOH, leading to low DOX leakage under physiological conditions particularly for the carboxyl functionalized material.

To release DOX from MCM-41-DOX-P[5]A and MCM-41-COO-DOX-P[5]A, the pH was adjusted from 7.4 (physiological pH) to 5.5 (lysosomal pH) and 2.0 by adding calculated volumes of dilute HCl. These studies were carried out at 37 °C (body temperature) and the absorption band of DOX at 483 nm in the UV-vis spectrum was monitored over time (Fig. S17, ESI†). As shown in Fig. 2, under acidic conditions the silanolate (MCM-41) or carboxylate groups (MCM-41-COO⁻) are protonated, and the electrostatic interactions with cationic P[5]A are weakened, opening the nanogate.

Fig. 3 shows the DOX release profiles as percentages *versus* time. At physiological pH (7.4), 37 °C (Fig. 3) and before HCl addition, MCM-41-DOX-P[5]A and MCM-41-COO-DOX-P[5]A are in the “gate-closed state”, and the DOX leakage monitored within 2 h was only 4.1 and 1.7%, respectively. After 2 h, HCl was added to the cuvette to reach pH = 5.5 or 2.0. At this point, the nanocarriers immediately switched to the “gate-open state” and a burst release of DOX was detected (Fig. 3 and Fig. S17, ESI†). The kinetics is faster in the first stages of DOX release for both nanocarriers at both pH values. At acid pH values, the silanolate or carboxylate conjugate bases of MCM-41 and MCM-41-COO⁻ are immediately protonated and the equilibrium shifts towards the nonionized acid form (silanol and carboxyl groups). The outcome is that the P[5]A molecules located on the surface of MCM-41 promptly dissociate and DOX is released. However, at pH = 2.0 the equilibrium is reached more quickly for MCM-41-DOX-P[5]A and the percentage of DOX released from this nanocarrier (59%) is smaller than that released by MCM-41-COO-DOX-P[5]A (91%) in the same period of time (30 h) (Fig. 3). We can explain the behavior of MCM-41-DOX-P[5]A based on the results in Fig. 2, which shows that P[5]A is not totally removed from the DOX-unloaded MCM-41-P[5]A nanocarrier, most likely because part of the P[5]A is interacting with silanolate groups inside the pores of MCM-41, making them less accessible for protonation.

Therefore, due to the lower release of DOX from MCM-41-DOX-P[5]A compared to MCM-41-COO-DOX-P[5]A, the next studies were carried out using the latter system.

Acid- and base-driven chemical switching of MCM-41-COO-DOX-P[5]A

To demonstrate that P[5]A behaves as a switchable nanogate in MCM-41-COO-DOX-P[5]A which can be turned on and off to regulate the passage of DOX through the nanochannels of MCM-41 functionalized with carboxyl groups, we carried out an experiment based on the reversibility of the acid–base equilibrium between the carboxyl group (MCM-41-COOH) and the carboxylate anion (MCM-41-COO⁻). We have already demonstrated that the cationic stopper P[5]A

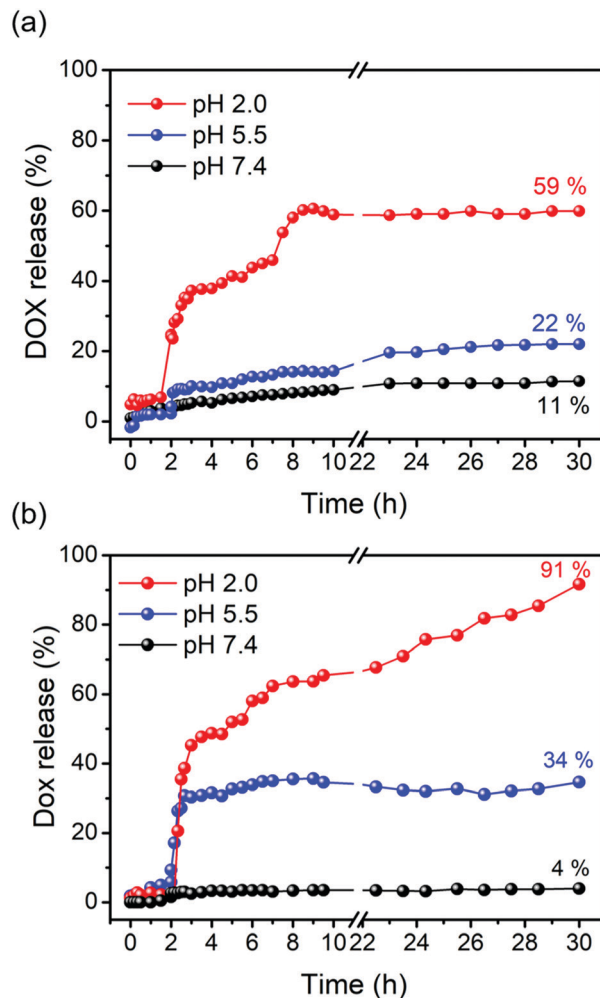


Fig. 3 Acid-triggered release profiles of DOX in PBS from (a) MCM-41-DOX-P[5]A and (b) MCM-41-COO-DOX-P[5]A at 37 °C as a function of time.

electrostatically interacts with the negatively charged surface of MCM-41-COO⁻ (Fig. 1). With addition of acid (pH = 5.5 or 2.0) the carboxylate groups are protonated and the attractive coulombic forces are broken, releasing the stopper and drug simultaneously.

Bases that can deprotonate the carboxyl groups of MCM-41-COOH could act as chemical inputs, regenerating the electrostatic interaction between P[5]A and MCM-41-COO⁻ and ceasing the release of DOX from the nanochannels of the MSNPs. Therefore, the chemical switching of the nanogate was investigated by successive additions of HCl to a suspension of MCM-41-COO-DOX-P[5]A in PBS (pH = 7.4) to reach pH 5.5 or 2.0 and then addition of NaOH to return to pH 7.4 (Fig. 4). Upon addition of calculated volumes of 3.0 mol L⁻¹ HCl to the dispersion in PBS (the pH changes from 7.4 to 5.5 or 2.0, first point of the curve in Fig. 4) the nanogate is turned on, and DOX is immediately released (Fig. 4 and Fig. S18, ESI†). Subsequently, the nanogate is turned off by adjusting the pH to 7.4 through the addition of a NaOH solution (3.0 mol L⁻¹). In this state, the nanogate is closed, and the DOX release ceases; *e.g.*, the percentage of DOX released remains almost constant. The switching process was repeated eight times, proving that

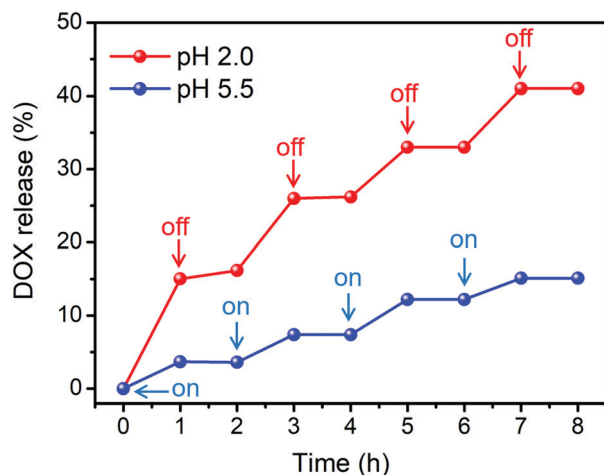


Fig. 4 DOX release profiles as a function of time from MCM-41-COO-DOX-P[5]A after consecutive additions of acid and base to a suspension of the nanocarrier in PBS at 37 °C.

MCM-41-COO-DOX-P[5]A operates almost reversibly. In theory, the reversibility of the switching mechanism allows this nanocarrier to be reloaded with DOX in the gate-open state, re-locked in the gate-closed state and reused at least eight times.

Investigation of competitive binding using citrate³⁻ and Zn²⁺

The following experiments were carried out to investigate the effect of some ionic species which are present in the blood on the nanogate operation. There is a myriad of ionic species that could affect the nanogate operation leading to premature release of the drug before reaching the target, and it would be impossible to investigate all of them. Therefore, we choose to investigate the effect of some ionic species present at considerable concentrations in the blood, such as citrate³⁻ and Zn²⁺.

High levels of citrate ions are naturally present in most healthy cells due to their vital importance in the Krebs cycle or citric acid cycle.^{66–68} In the blood, citrate acid exists predominantly as a trivalent anion (citrate³⁻) at high concentrations (ca. 100–135 $\mu\text{mol L}^{-1}$) and can be taken up from the blood *via* transporters found in many different organs, such as the kidneys, intestine, liver, placenta and brain.^{68–70} Therefore, at pH 7.4 the citrate anion could compete with the carboxylate groups anchored on the surface of MCM-41-COOH leading to undesirable release of DOX in the blood and in healthy cells. To check if citrate anions can trigger DOX release from MCM-41-COO-DOX-P[5]A, we added sodium citrate (19 mmol L^{-1}) to a MCM-41-COO-DOX-P[5]A dispersion in PBS buffer. In the first two hours of the experiment, no citrate was added and a minimum amount of DOX was released as previously discussed (Fig. 3). After this period, sodium citrate was added and only 5% of DOX was released at pH 7.4 (Fig. 5 and Fig. S19, ESI[†]).

In addition, the human body has several metal ions which are essential for organism functioning. Among them, Zn²⁺ plays vital biological roles,^{71,72} and can be found in organs, tissues, cytoplasm and blood either as a free ion or bound to proteins.

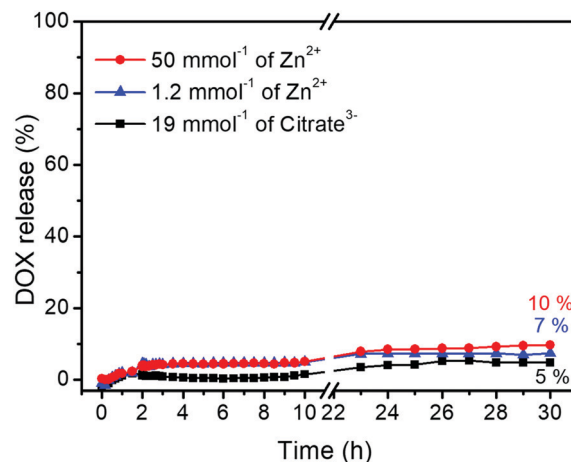


Fig. 5 The release profiles of DOX from MCM-41-COO-DOX-P[5]A in the presence of citrate³⁻ (19 mmol L^{-1}) and Zn²⁺ (1.2 and 50 mmol L^{-1}) in PBS buffer solutions at 37 °C.

The concentrations of Zn²⁺ are in the range of nano to picomolar depending on the type of tissue and methodology of analysis.^{72–74} Because the surface of the mesoporous silica contains carboxylate groups, Zn²⁺ could compete with P[5]A by these negative groups and turn-on the nanogate, leading to premature release. Fig. 5 and Fig. S19 (see the ESI[†]) show the release profiles of DOX from MCM-41-COO-DOX-P[5]A in water upon addition of Zn²⁺ at two concentrations (1.2 and 50 mmol L^{-1}). The release of DOX to the solution using 1.2 mmol L^{-1} and 50 mmol L^{-1} was 7 and 10%, respectively. Therefore, Zn²⁺ cations are not able to efficiently open the nanogate. Most likely, there is an electrostatic repulsion between Zn²⁺ cations and the positive surface of the nanogate in MCM-41-COO-DOX-P[5]A (see the ζ -potential values in Fig. 1), preventing Zn²⁺ binding to carboxylate groups anchored on the surface of MCM-41.

Therefore, neither citrate³⁻ nor Zn²⁺ at the investigated concentrations were able to efficiently open the nanogate, which is an interesting result for practical applications because the undesirable release of DOX in the presence of these ions in the blood would decrease the ability of the nanocarrier to treat cancer cells and also could lead to side effects.

In vitro cytotoxicity assays and cellular uptake of DOX-unloaded MCM-41-COO-P[5]A and DOX-loaded MCM-41-COO-DOX-P[5]A and free DOX

The cell viability of MCF-7 cells (human breast adenocarcinoma cell line) upon treatment with DOX-loaded and DOX-unloaded MCM-41-COO-P[5]A and free DOX was assessed. The DOX-unloaded nanocarrier was incubated at concentrations of 23.25, 46.50, 116.28 or 232.56 $\mu\text{g mL}^{-1}$ (Fig. S20, ESI[†]), which correspond to DOX concentrations in the MCM-41-COO-DOX-P[5]A nanocarrier of 0.5, 1.0, 2.5, and 5.0 $\mu\text{g mL}^{-1}$, respectively. The cell viability of free DOX was evaluated at the same concentrations for comparison.

The incubation of MCF-7 cells with DOX-unloaded MCM-41-COO-P[5]A showed some cellular response with a maximum decrease of about 50% in cell viability related to the control cells in both 24 and 48 h of incubation time (Fig. 6a and b and Fig. S20, ESI[†]). However, the impact on MCF-7 viability was

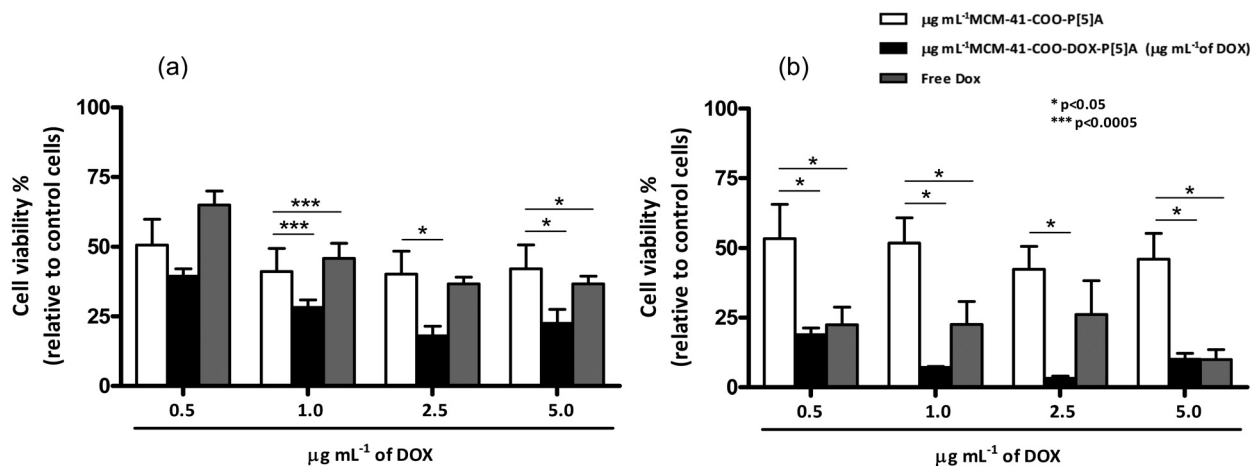


Fig. 6 MTT viability assay of MCF-7 cells treated with DOX-unloaded MCM-41-COO-P[5]A or DOX-loaded MCM-41-COO-DOX-P[5]A or free DOX for (a) 24 h and (b) 48 h. To reach concentrations of 0.5, 1.0, 2.5 and 5.0 $\mu\text{g mL}^{-1}$ of DOX in the nanocarrier 23.25, 46.50, 116.28 or 232.56 $\mu\text{g mL}^{-1}$ of MCM-41-COO-DOX-P[5]A was used.

neither time- nor concentration-dependent, suggesting that the phenomenon observed might be due to an initial protective cellular response rather than a cytotoxic effect of the DOX-unloaded MCM-41-COO-P[5]A system. In contrast, incubation of MCF-7 cells with increasing concentrations of DOX-loaded MCM-41-COO-DOX-P[5]A revealed a progressive decrease of cell viability from 40% (0.5 $\mu\text{g mL}^{-1}$ of DOX) to 25% (5.0 $\mu\text{g mL}^{-1}$ of DOX) in 24 h and from 18% (0.5 $\mu\text{g mL}^{-1}$ of DOX) to 10% (5.0 $\mu\text{g mL}^{-1}$ of DOX) in 48 h of treatment (Fig. 6a and b). Therefore, the MCF-7 treatment with the DOX-loaded MCM-41-COO-DOX-P[5]A induces concentration and time-dependent cytotoxicity. The lowest cell viability was obtained using 2.5 $\mu\text{g mL}^{-1}$ of DOX loaded in the MCM-41-COO-DOX-P[5]A nanocarrier. Importantly, the cell viability of the DOX-loaded MCM-41-COO-DOX-P[5]A was lower than that of free DOX at all concentrations investigated.

Most likely, the cytotoxicity improvement caused by the DOX-loaded MCM-41-COO-DOX-P[5]A in comparison with free DOX might be due to higher cellular uptake through endocytosis compared to passive diffusion of free DOX.^{75,76}

The MCF-7 cell uptake of MCM-41-COO-DOX-P[5]A and free DOX after incubation for 4 and 24 h was also investigated (Fig. 7). The internalization and location of DOX are indicated by its red fluorescence. The MCF-7 cell images incubated with free DOX at concentrations of 1.0 and 5.0 $\mu\text{g mL}^{-1}$ show that DOX is mainly localized in the nucleus of the cells after 4 and 24 h of incubation. Upon treatment of MCF-7 cells with DOX-loaded MCM-41-COO-DOX-P[5]A nanocarrier concentrations of 46.50 and 232.56 $\mu\text{g mL}^{-1}$, which correspond to 1.0 and 5.0 $\mu\text{g mL}^{-1}$ of DOX, respectively, for 4 h, one can see that DOX is distributed between the cell membrane and the nucleus

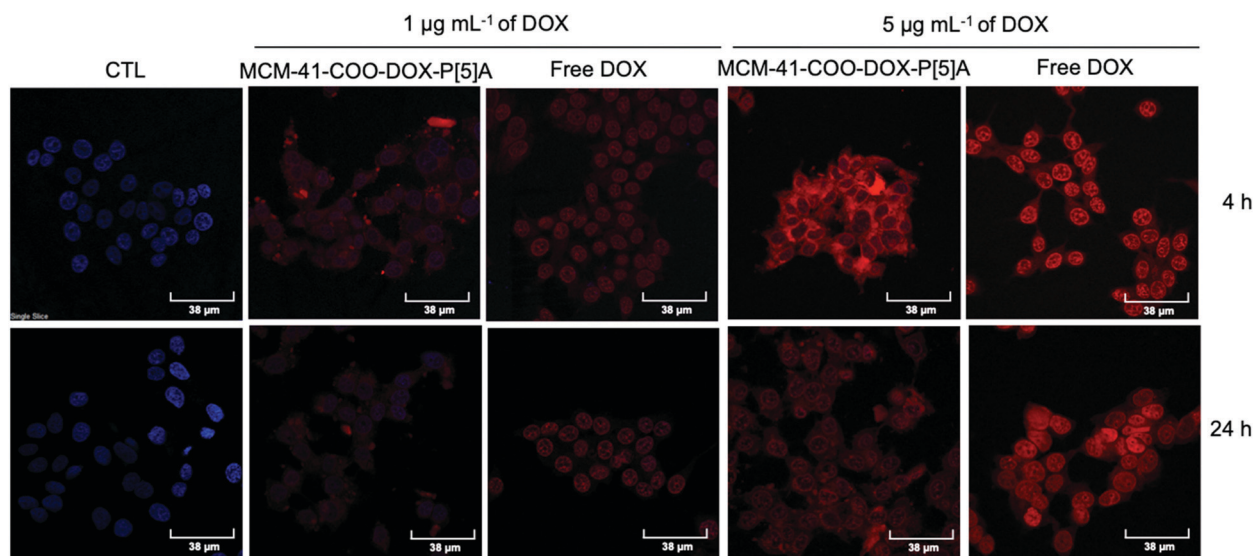


Fig. 7 Confocal fluorescence microscopy images of MCF-7 cells at 37 °C treated with MCM-41-COO-DOX-P[5]A (containing 1.0 and 5.0 $\mu\text{g mL}^{-1}$ of DOX) and free DOX (1.0 and 5.0 $\mu\text{g mL}^{-1}$) for 4 h and 24 h. Red fluorescence: DOX. Blue fluorescence: DAPI (nuclear staining).

(labelled with blue fluorescence). After 24 h of treatment, the drug is mainly detected inside the nucleus of the cells, suggesting that MCM-41-COO-DOX-P[5]A is internalized by the MCF-7 cells.

Conclusions

In conclusion, we have designed and constructed a novel pH-responsive nanocarrier loaded with DOX by integrating negatively charged mesoporous silica nanoparticles and a water-soluble cationic pillar[5]arene (P[5]A) nanogate through electrostatic interactions between the silanolate groups of MCM-41 (MCM-41-DOX-P[5]A) or carboxylate groups anchored on the surface of MCM-41 (MCM-41-COO-DOX-P[5]A) and P[5]A. SEM and TEM images revealed spherical particles with a narrow size distribution and parallel nanochannels of MCM-41 and MCM-41-COOH synthesized in this work. The interactions between the quaternary ammonium moieties of P[5]A and the carboxylate or silanolate groups on the mesoporous silica nanoparticles were demonstrated by ζ -potential measurements at different pH values. P[5]A was efficient as a nanogate to block the entrapped drug in the nanochannels of the MSNPs under physiological conditions. However, for MCM-41-DOX-P[5]A, P[5]A is trapped inside the nanochannels even under very acidic conditions, and the nanogate is not completely released. At pH 2.0, the amount of DOX released is higher than at pH 5.5 for both nanocarriers. In addition, MCM-41-COO-DOX-P[5]A showed potential smart on-off release behaviour because of the reversible nature of the electrostatic interactions. Ionic species such as citrate³⁻ and Zn²⁺ did not show a significant effect on the nanogate operation at the investigated concentrations. *In vitro* experiments showed that the cell viability of DOX-unloaded MCM-41-COO-P[5]A was neither time- nor concentration-dependent. DOX-loaded MCM-41-COO-DOX-P[5]A presented a higher cytotoxic effect than free DOX at the same concentration. Confocal fluorescence microscopy revealed that the nanocarrier was capable of releasing DOX in the cell nucleus. Therefore, this novel nanocarrier appears to be a potential candidate to be envisioned as an alternative system for cancer therapy; however, additional studies could be very useful to further evaluate its anticancer potential.

Experimental

Chemicals

Hexadecyltrimethylammonium bromide (CTAB) (99%), tetraethyl orthosilicate (TEOS) (99%), 3-cyanopropyltriethoxysilane (CyPTES) ($\geq 98\%$), triphenylphosphine (99%), tetrabromomethane (PA), hydroquinone bis(2-hydroxyethyl)ether (99%), trimethylamine (35%), paraformaldehyde (PA), boron trifluoride diethyl etherate (PA), doxorubicin chloride (98%), sodium bicarbonate (NaHCO₃) (99.7%), sodium sulfate (Na₂SO₄) (99%), potassium chloride (KCl) (99%), sodium chloride (NaCl) (99%), ammonium chloride (NH₄Cl) (98%), sodium phosphate dibasic (Na₂HPO₄) (98%), potassium phosphate monobasic (NaH₂PO₄) (98%), zinc chloride (ZnCl₂) (98%), sodium citrate (99%) and 3-(4,5-dimethylthiazol-2-yl)-2,5-diphenyltetrazolium bromide (MTT) were purchased from Sigma-Aldrich and used as received. All necessary solvents and

hydrochloric acid (HCl) (37% PA), sulfuric acid (H₂SO₄) (98% PA) and sodium hydroxide (NaOH) ($\geq 99\%$) were purchased from Vetec.

Characterization

¹H and ¹³C NMR spectra of the quaternary ammonium pillar[5]arene salt were recorded on a Varian VNMRS at 500 MHz and 75 MHz, respectively, using residual solvent as an internal standard. The sample was prepared using D₂O purchased from Cambridge Isotope Laboratories.

A PerkinElmer CHN 240 C analyser at the Analytical Center of the Institute of Chemistry, University of São Paulo, Brazil, was used to determine the carbon, hydrogen and nitrogen contents of the MCM-41-CN and MCM-41-COOH samples.

Fourier transform infrared (FTIR) spectra were acquired using a Thermo Nicolet iS50 FTIR instrument.

Raman spectra were recorded on a Bruker MultiRAM FT-Raman spectrometer (Bruker, Germany) equipped with a neodymium-doped yttrium aluminium garnet (Nd:YAG) laser excitation source operating at $\lambda_{\text{Nd:YAG}} = 1064$ nm and a germanium detector. The samples were placed on the hemispheric bore of an aluminium sample holder, and the spectra were acquired over the range of 4000–500 cm⁻¹ at room temperature with 128 scans at a laser power of 300 mW. The spectral resolution was 2 cm⁻¹.

Powder X-ray diffraction (PXRD) data of the samples were collected on a Rigaku Miniflex II X-ray diffractometer with CuK α ($\lambda = 1.5418$ Å) within 1.5 and 7° of 2θ .

Textural analysis was carried out on a Micromeritics ASAP 2020 V304-4 serial 1200 apparatus by determining the N₂ adsorption/desorption isotherms at 77 K. Before the analysis, the samples were heated up to 100 °C at a rate of 1 °C min⁻¹ under a vacuum. The Brunauer–Emmett–Teller (BET) and Barrett–Joyner–Halenda (BJH) methods were used to assess the specific surface area and pore size distribution, respectively.

The dynamic light scattering (DLS) size and the zeta potential (ζ -potential) were measured using a ZetaPlus Zeta Potential Analyzer by Brookhaven Instruments Corporation.

The morphological characterization of MCM-41 and MCM-41-COOH was performed using Scanning Electron Microscopy (SEM) and High-Resolution Transmission Electron Microscopy (HRTEM). HRTEM images were acquired on a JEOL 2100F instrument operated at an accelerating voltage of 200 kV and a current of 130 μ A and equipped with a CCD camera (GATAN Orius, 11 Mpixel). SEM images were acquired on a field emission JEOL 7100FT instrument operated at 8 kV with a work distance of 9.9 mm and spot size of 8 mm. The samples were prepared by dropping a sonicated (30 min) ethanolic dispersion (0.5 mg mL⁻¹) of MCM-41 or MCM-41-COOH onto a copper grid with a carbon film coating (Ted Pella) and Si substrates for HRTEM and SEM analyses, respectively. Then, the grid and Si substrate were dried at 50 °C for 24 h before analysis. The particle distribution from SEM images was obtained by measuring the diameter of about 200 particles using the ImageJ software.

UV-vis absorption spectra were acquired using a Cary 60 UV-vis spectrophotometer (Varian). A thermoelectric (Peltier system) cuvette holder (TLC 40) coupled with a temperature controller (Quantum Northwest TC 125) was used to keep the

temperature of MCM-41-COO-DOX-P[5]A and MCM-41-DOX-P[5] dispersions at 37 °C during DOX release experiments.

Synthesis of the quaternary ammonium pillar[5]arene salt (P[5]A)

The synthesis of the quaternary ammonium pillar[5]arene salt was carried out as described in the literature with minor modifications.³⁹ Under stirring and a N₂ atmosphere, tetrabromomethane (23.81 mmol) was slowly added to a mixture containing hydroquinone bis(2-hydroxyethyl)ether (10 mmol) and triphenylphosphine (21.81 mmol) in 50 mL of dry acetonitrile at 0 °C. After the reaction mixture reached room temperature, it was stirred for an additional 4 h. Then, 40 mL of cold water was added; the product precipitated as a white solid and was collected by vacuum filtration, washed 3 times with methanol/water and then recrystallized from methanol. The white crystals were dried under a vacuum, yielding compound **1** (90%) as a white solid. The compound was characterized by ¹H and ¹³C NMR, and the data obtained are in agreement with the literature.⁷⁷ To a solution of compound **1** in dichloromethane (230 mL), paraformaldehyde (30.87 mmol) and boron trifluoride diethyl etherate (33.86 mmol) were added under a N₂ atmosphere, and the solution was stirred at room temperature for 2 h. Then, the reaction mixture was washed with water, saturated sodium bicarbonate solution and brine, and the organic layer was dried over anhydrous sodium sulfate and concentrated under a vacuum. The residue was purified by chromatography on silica gel using dichloromethane/hexane (27:23) as the eluent, yielding 66% compound **2** as a white solid. The compound was characterized by ¹H and ¹³C NMR, and the data obtained are in agreement with the literature.⁷⁷ To a solution of compound **2** (1.19 mmol) in ethanol (100 mL), trimethylamine (48.11 mmol) was added, and the reaction was stirred overnight under reflux. Then, the mixture was filtered under a vacuum, and the solid obtained was washed with ethanol. The product was dried under a vacuum, yielding compound P[5]A (95%). Mp: 101–103 °C. ¹H NMR (D₂O, RT, 500 MHz) of P[5]A (ppm): 7.03 (s, 10H), 4.53 (s, 20H), 4.02 (s, 10H), 3.88 (s, 20H), 3.31 (s, 90H). ¹³C NMR (D₂O, RT, 75 MHz) (ppm): 149.43, 129.97, 116.54, 64.93, 63.50, 54.08 and 29.54.

Synthesis of MCM-41-CTAB

The synthesis of MCM-41 was carried out following the procedure described by Zink *et al.* with minor modifications.^{40–42} CTAB (1.0 g) was added to a solution of NaOH in deionized water (DI) (14.5 mmol L⁻¹, 967 mL) under vigorous stirring. Subsequently, the solution was heated at 80 °C for 30 min and after this period TEOS (10 mL) was added dropwise for approximately 3 min. Then, the reaction mixture remained at 80 °C for 2 h. The reaction mixture was cooled to room temperature (RT), filtered, washed with DI water (2×) and EtOH (1×) and dried overnight under air, yielding a white solid named MCM-41-CTAB (3.0 g).

Extraction of the organic template from MCM-41-CTAB

To extract the organic template from the pores, MCM-41-CTAB (300 mg) was dispersed in an ethanolic solution of NH₄Cl (5.0 g, 300 mL) under vigorous stirring and then the dispersion

remained under reflux for 2 h. The solid was collected by filtration, and washed with hot DI water (2×) and EtOH (1×). The organic template extraction procedure was repeated one more time to remove CTAB completely from the MCM-41 pores, and then the product was dried yielding a white solid (180 g).

Preparation of carboxyl-functionalized MCM-41 (MCM-41-COOH)

The mesoporous MCM-41 modification with carboxyl groups was carried out as described using a methodology employed by our group to modify silica nanoparticles with various functional groups.^{17,18,43–49} However, in the procedure used in this work, the organic template was removed after functionalization with 3-cyanopropyl groups. For the functionalization, 2.5 mL of CyPTES was added dropwise to a suspension of MCM-41-CTAB (544 mg) in anhydrous PhMe (200 mL) under reflux in a N₂ atmosphere, while stirring vigorously. After 2.0 h, a fraction of 2.0 mL of PhMe containing EtOH was distilled off from the suspension, followed by the addition of 1.5 mL more of CyPTES. The reaction mixture was left to stir under reflux in a N₂ atmosphere for an additional 24 h. The solid was collected by filtration, washed with anhydrous PhMe (1×) and EtOH (1×) and dried overnight under air. The obtained material was dispersed in an ethanolic solution of NH₄Cl (5.0 g, 300 mL) under vigorous stirring and then the dispersion remained under reflux for 2 h. After this period, the solid was filtered, washed with hot DI water (2×) and EtOH (1×) and dried overnight under air. For the hydrolysis of the 3-cyanopropyl groups, the obtained solid was slowly dispersed in 100 mL of a 30% H₂SO₄ solution (v/v) under stirring. The suspension was left to stir under reflux for 4 h and the resulting solid was then collected by filtration, washed with DI water (up to pH = 7) and dried under a vacuum at RT for 8 h to afford MCM-41-COOH (223 mg).

Potentiometric titration of MCM-41 and MCM-41-COOH

First, 10.0 mg of MCM-41 or 10 mg of MCM-41-COOH was dispersed in 10 mL of degassed deionized water by sonication for 30 min, and then the dispersion was titrated with 19.86 mmol L⁻¹ NaOH. The pH of the dispersion was registered using a pH meter (pH 300 M). The pK_a constants of MCM-41 and MCM-41-COOH were obtained by the Gran titration method.^{59,60}

MCM-41 and MCM-41-COOH DOX-loading and closing with P[5]A

64 mg of MCM-41 or MCM-41-COOH was dispersed in 30 mL of phosphate buffered saline solution (PBS, pH = 7.4) containing 32.2 mg L⁻¹ of DOX. The dispersions were light protected and stirred for 72 h at RT. Then, 32 mg of P[5]A was added to each dispersion, and the mixtures were stirred for 24 h at RT. The excess of DOX and P[5]A were removed from the resulting materials through successive centrifugation and washing steps. The solids were collected and dried under a vacuum at RT for 8 h, resulting in MCM-41-DOX-P[5]A and MCM-41-COO-DOX-P[5]A. The amount of DOX loaded into the nanochannels of

MCM-41 or MCM-41-COOH capped by P[5]A was determined by a UV-vis standard curve that was created by measuring a series of concentrations of DOX solutions in PBS at $\lambda = 483$ nm. The DOX-loading efficiency was calculated using eqn (1), where M is the initial mass of DOX (1.94 mg) in the solution and m is the loaded DOX mass per 100 mg of MCM-41-COOH or MCM-41. The DOX-loading efficiency for MCM-41 and MCM-41-COOH was 52.4% and 57.6%, respectively.

$$\text{DOX-loading efficiency (\%)} = m/M \times 100. \quad (1)$$

DOX controlled release studies

The controlled release of DOX and P[5]A from MCM-41-DOX-P[5]A and MCM-41-COO-DOX-P[5]A was investigated at different pH values (2.0, 5.5 and 7.4) or with adding ZnCl_2 (1.2 and 50 mmol L^{-1}) or sodium citrate (19 mmol L^{-1}) at 37 °C by UV-vis spectroscopy. All DOX and P[5]A release experiments were performed by transferring 1 mg of MCM-41-DOX-P[5]A or MCM-41-COO-DOX-P[5]A to a quartz cuvette containing a small magnetic stir bar and adding 2 mL of a PBS solution (pH = 7.4). The cuvettes were placed into a thermoelectrically controlled cuvette holder adjusted to 37 °C and gently stirred. After the decantation of the solid, UV-vis spectra were recorded at different time intervals up to 30 h. The DOX and P[5]A release was triggered by changing the pH of the PBS suspension (pH = 7.4) to 5.5 and 2.0 by adding calculated volumes of HCl solution (3.0 mol L^{-1}).

Chemical switching experiments (ON-OFF)

The changes in the absorbance of DOX were observed at 483 nm for MCM-41-COO-DOX-P[5]A (1 mg) dispersed in a PBS solution (2 mL) upon the successive addition of calculated volumes of acid (3.0 mol L^{-1} HCl) to reach pH 5.5 or 2.0 and base (NaOH 3.0 mol L^{-1}) to return to pH 7.4. The dilutions were considered to calculate the final concentrations of DOX.

Cell lines and treatments

Human breast adenocarcinoma cells (MCF-7) were obtained from the Laboratory of Cellular and Molecular Hemato-Oncology of the Brazilian National Cancer Institute and cultured in Dulbecco's modified Eagle's medium (DMEM) (Sigma) containing 10% fetal bovine serum (FBS) and 1% penicillin/streptomycin/glutamine (Invitrogen) at 37 °C under 5% CO_2 . Doxorubicin hydrochloride was added to the culture medium of exponentially growing cells at increasing concentrations and time periods. 3-(4,5-Dimethylthiazol-2-yl)-2,5-diphenyltetrazolium bromide (MTT) was also added to the cell culture medium.

In vitro cellular uptake

For the cellular uptake of DOX-loaded MCM-41-COO-DOX-P[5]A and free doxorubicin (DOX) MCF-7 cells (9×10^3 cells per well) were grown on coverslips in a 24-well plate with 500 μL of DMEM (supplemented with 10% FBS and 1% penicillin/streptomycin/glutamine) for 24 h at 37 °C under 5% CO_2 . Then, the cells were rapidly washed with PBS (pH 7.4), and the culture medium was replaced by fresh medium containing 1.0 or

5.0 $\mu\text{g mL}^{-1}$ of either free DOX or MCM-41-COO-DOX-P[5]A (suspended in PBS, pH 7.4). After treatment for 4 or 24 h, the cells were washed with PBS (pH 7.4) and fixed with paraformaldehyde (4%), and the nuclei were stained with DAPI (4',6-diamidino-2-phenylindole) (Vectashield). Subsequently, the samples were assessed using confocal laser-scanning microscopy (CLSM, Olympus Fluoview FV 10i, Tokyo, Japan). Analyses were performed in three independent experiments (DOX: $\lambda_{\text{ex}} = 559$; $\lambda_{\text{em}} = 570$ –670 nm and DAPI: $\lambda_{\text{ex}} = 359$; $\lambda_{\text{em}} = 461$ nm).

In vitro cytotoxicity assay

MCF-7 cells (9×10^3 per well) were seeded in a 96-well plate and cultured in 200 μL of DMEM (supplemented with 10% FBS and 1% penicillin/streptomycin/glutamine) for 24 h at 37 °C under a humidified 5% CO_2 atmosphere. Next, the culture medium was discarded, and the cells were washed with PBS (pH 7.4). Then, fresh medium was added with one of the different treatments (free DOX or MCM-41-COO-DOX-P[5]A) at DOX concentrations of 0.5, 1.0, 2.5 or 5.0 $\mu\text{g mL}^{-1}$ and incubated for either 24 h or 48 h. Subsequently, the cells were washed with PBS (pH 7.4) and incubated with 100 μL of a 3-(4,5-dimethylthiazol-2-yl)-2,5-diphenyltetrazolium bromide (MTT) solution (0.5 $\mu\text{g mL}^{-1}$ in DMEM) for 2 h. Then, the MTT solution was removed, and the cells were lysed with 100 μL of DMSO. The absorption was measured at $\lambda = 570$ nm after automatic shaking for 40 s in a microplate reader (Molecular Devices, Spectra max 190, California, United States). To determine the biocompatibility of MCM-41-COO-P[5]A, MCF-7 cells were incubated with increasing amounts of this material (23.25, 46.50, 116.28 or 232.56 $\mu\text{g mL}^{-1}$) for 24 or 48 h, and the cell viability was evaluated by incubation with MTT, as described before. All determinations were performed in three independent experiments.

Conflicts of interest

There are no conflicts to declare.

Acknowledgements

The authors gratefully acknowledge the National Council for Scientific and Technological Development for the research grant (CNPq grant number 434141/2018-6 and 313799/2017-2) and fellowships of C. M. R. and L. F. R. P.; the Brazilian Federal Agency for the Support and Evaluation of Graduate Education (CAPES) for the fellowships of E. C. S. S., T. C. S. and T. S. F. and Pró-equipamentos, and the Rio de Janeiro Research Foundation for the fellowship of V. G. C. M and research projects (Faperj grant number E-26/010101133/2018 and E-26/202629/2019). We are grateful to the Material Characterization (<http://www.uff.br/lamate/>), Molecular Spectroscopy (<http://www.uff.br/lame/>), NMR (<http://www.laremn.uff.br/>), and Multiuser Laboratories from Universidade Federal Fluminense (UFF). The authors also would like to thank the Multiuser Laboratory of Nanoscience and Nanotechnology from Centro Brasileiro de Pesquisas Físicas (LABNANO-CBPF).

Notes and references

- 1 R. Sun, W. Wang, Y. Wen and X. Zhang, *Nanomaterials*, 2015, **5**, 2019–2053.
- 2 C. R. Thomas, D. P. Ferris, J.-H. Lee, E. Choi, M. H. Cho, E. S. Kim, J. F. Stoddart, J.-S. Shin, J. Cheon and J. I. Zink, *J. Am. Chem. Soc.*, 2010, **132**, 10623–10625.
- 3 J. S. F. Silva, J. Y. R. Silva, G. F. de Sá, S. S. Araújo, M. A. G. Filho, C. M. Ronconi, T. C. Santos and S. A. Júnior, *ACS Omega*, 2018, **3**, 12147–12157.
- 4 X. Huang and X. Z. Du, *ACS Appl. Mater. Interfaces*, 2014, **6**, 20430–20436.
- 5 E. Aznar, M. Oroval, L. Pascual, J. R. Murguía, R. Martínez-Mañez and F. Sancenón, *Chem. Rev.*, 2016, **116**, 561–718.
- 6 L.-B. Meng, W. Zhang, D. Li, Y. Li, X.-Y. Hu, L. Wang and G. Li, *Chem. Commun.*, 2015, **51**, 14381–14384.
- 7 X. Wu, Y. Li, C. Lin, X.-Y. Hu and L. Wang, *Chem. Commun.*, 2015, **51**, 6832–6835.
- 8 N. Song and Y.-W. Yang, *Chem. Soc. Rev.*, 2015, **44**, 3474–3504.
- 9 Z. Li, J. C. Barnes, A. Bosoy, J. F. Stoddart and J. I. Zink, *Chem. Soc. Rev.*, 2012, **41**, 2590–2605.
- 10 Y. Xu, Y. Zhu and S. Kaskel, *RSC Adv.*, 2015, **5**, 99875–99883.
- 11 B. Rühle, S. Datz, C. Argyo, T. Bein and J. I. Zink, *Chem. Commun.*, 2016, **52**, 1843–1846.
- 12 D. Tarn, D. P. Ferris, J. C. Barnes, M. W. Ambrogio, J. F. Stoddart and J. I. Zink, *Nanoscale*, 2014, **6**, 3335–3343.
- 13 C. D. Ding, Y. Liu, T. Wang and J. J. Fu, *J. Mater. Chem. B*, 2016, **4**, 2819–2827.
- 14 Y. Yao, Y. Wang, R. Zhao, L. Shao, R. Tang and F. Huang, *J. Mater. Chem. B*, 2016, **4**, 2691–2696.
- 15 P.-J. Chen, S.-H. Hu, C.-S. Hsiao, Y.-Y. Chen, D.-M. Liu and S.-Y. Chen, *J. Mater. Chem.*, 2011, **21**, 2535–2543.
- 16 Y.-L. Sun, Y. Zhou, Q.-L. Li and Y.-W. Yang, *Chem. Commun.*, 2013, **49**, 9033–9035.
- 17 G. Q. Silveira, R. S. Da Silva, L. P. Franco, M. D. Vargas and C. M. Ronconi, *Microporous Mesoporous Mater.*, 2015, **206**, 226–233.
- 18 G. Q. Silveira, M. D. Vargas and C. M. Ronconi, *J. Mater. Chem.*, 2011, **21**, 6034–6039.
- 19 T. D. Nguyen, K. C.-F. Leung, M. Liong, C. D. Pentecost, J. F. Stoddart and J. I. Zink, *Org. Lett.*, 2006, **8**, 3363–3366.
- 20 Y. Zhou, L.-L. Tan, Q.-L. Li, X.-L. Qiu, A.-D. Qi, Y. Tao and Y.-W. Yang, *Chem. – Eur. J.*, 2014, **20**, 2998–3004.
- 21 Z. Tong, J. Zhou, R. Huang, J. Zhou, R. Zhang, W. Zhuo and G. Jiang, *J. Polym. Sci., Part A: Polym. Chem.*, 2017, **55**, 2477–2482.
- 22 T. Ogoshi, S. Kanai, S. Fujinami, T.-A. Yamagishi and Y. Nakamoto, *J. Am. Chem. Soc.*, 2008, **130**, 5022–5023.
- 23 T. Ogoshi and T. Yamagishi, *Chem. Commun.*, 2014, **50**, 4776–4787.
- 24 P. J. Cragg and K. Sharma, *Chem. Soc. Rev.*, 2012, **41**, 597–607.
- 25 M. Xue, Y. Yang, X. Chi, Z. Zhang and F. Huang, *Acc. Chem. Res.*, 2012, **45**, 1294–1308.
- 26 T. S. Fernandes, E. C. S. Santos, V. G. C. Madriaga, V. Nascimento, F. Garcia and C. M. Ronconi, *J. Braz. Chem. Soc.*, 2019, **30**, 2452–2463.
- 27 T. Ogoshi, M. Hashizume, T. Yamagishi and Y. Nakamoto, *Chem. Commun.*, 2010, **46**, 3708–3710.
- 28 N. Song, T. Kakuta, T. Yamagishi, Y.-W. Yang and T. Ogoshi, *Chem*, 2018, **4**, 2029–2053.
- 29 X.-Y. Lou, Y.-P. Li and Y.-W. Yang, *Biotechnol. J.*, 2018, **14**, 1800354.
- 30 X. Wu, Y. Zhang, Y. Lu, S. Pang, K. Yang, Z. Tian, Y. Pei, Y. Qu, F. Wang and Z. Pei, *J. Mater. Chem. B*, 2017, **5**, 3483–3487.
- 31 Y.-L. Sun, Y.-W. Yang, D.-X. Chen, G. Wang, Y. Zhou, C.-Y. Wang and J. F. Stoddart, *Small*, 2013, **9**, 3224–3229.
- 32 X. Wang, L.-L. Tan, X. Li, N. Song, Z. Li, J.-N. Hu, Y.-M. Cheng, Y. Wang and Y.-W. Yang, *Chem. Commun.*, 2016, **52**, 13775–13778.
- 33 H. Li, R. Wei, G.-H. Yan, J. Sun, C. Li, H. Wang, L. Shi, J. A. Capobianco and L. Sun, *ACS Appl. Mater. Interfaces*, 2018, **10**, 4910–4920.
- 34 L.-L. Tan, H. Li, Y.-C. Qiu, D.-X. Chen, X. Wang, R.-Y. Pan, Y. Wang, S. X.-A. Zhang, B. Wang and Y.-W. Yang, *Chem. Sci.*, 2015, **6**, 1640–1644.
- 35 L.-L. Tan, H. Li, Y. Zhou, Y. Zhang, X. Feng, B. Wang and Y.-W. Yang, *Small*, 2015, **11**, 3807–3813.
- 36 X. Huang, S. Wu, X. Ke, X. Li and X. Du, *ACS Appl. Mater. Interfaces*, 2017, **9**, 19638–19645.
- 37 Q.-L. Li, Y. Sun, L. Ren, X. Wang, C. Wang, L. Li, Y.-W. Yang, X. Yu and J. Yu, *ACS Appl. Mater. Interfaces*, 2018, **10**, 29314–29324.
- 38 M.-X. Wu, J. Gao, F. Wang, J. Yang, N. Song, X. Jin, P. Mi, J. Tian, J. Luo, F. Liang and Y.-W. Yang, *Small*, 2018, **14**, 1704440.
- 39 Y. Ma, X. Ji, F. Xiang, X. Chi, C. Han, J. He, Z. Abliz, W. Chen and F. Huang, *Chem. Commun.*, 2011, **47**, 12340–12342.
- 40 W. Chen, C.-A. Cheng, B.-Y. Lee, D. L. Clemens, W.-Y. Huang, M. A. Horwitz and J. I. Zink, *ACS Appl. Mater. Interfaces*, 2018, **10**, 31870–31881.
- 41 B. Rühle, D. L. Clemens, B.-Y. Lee, M. A. Horwitz and J. I. Zink, *J. Am. Chem. Soc.*, 2017, **139**, 6663–6668.
- 42 W.-Y. Huang and J. I. Zink, *J. Phys. Chem. C*, 2016, **120**, 23780–23787.
- 43 E. C. S. Santos, T. C. dos Santos, R. B. Guimarães, L. Ishida, R. S. Freitas and C. M. Ronconi, *RSC Adv.*, 2015, **5**, 48031–48038.
- 44 M. R. Mello, D. Phanon, G. Q. Silveira, P. L. Llewellyn and C. M. Ronconi, *Microporous Mesoporous Mater.*, 2011, **143**, 174–179.
- 45 A. L. de Lima, C. M. Ronconi and C. J. A. Mota, *Catal. Sci. Technol.*, 2016, **6**, 2877–2891.
- 46 T. C. dos Santos, S. Bourrelly, P. L. Llewellyn, J. W. M. Carneiro and C. M. Ronconi, *Phys. Chem. Chem. Phys.*, 2015, **17**, 11095–11102.
- 47 A. L. de Lima, J. S. C. Vieira, C. M. Ronconi and C. J. A. Mota, *Mol. Catal.*, 2018, **458**, 240–246.
- 48 G. Q. Silveira, C. M. Ronconi, M. D. Vargas, R. A. S. San Gil and A. Magalhães, *J. Braz. Chem. Soc.*, 2011, **22**, 961–967.
- 49 A. L. de Lima, A. Mbengue, R. A. S. San Gil, C. M. Ronconi and C. J. A. Mota, *Catal. Today*, 2014, **226**, 210–216.

- 50 T. C. Dos Santos and C. M. Ronconi, *Rev. Virtual Quím.*, 2014, **6**, 112–130.
- 51 B. A. Morrow and A. J. Mcfarlan, *J. Phys. Chem.*, 1992, **96**, 1395–1400.
- 52 G. Su, C. Yang and J.-J. Zhu, *Langmuir*, 2015, **31**, 817–823.
- 53 B. Schrader and D. Bougeard, *Infrared and Raman Spectroscopy: Methods and Applications*, VCH, Weinheim, 1995.
- 54 L. G. Thygesen, M. M. Lokke, E. Micklander and S. B. Engelsen, *Trends Food Sci. Technol.*, 2003, **14**, 50–57.
- 55 S. Fiorilli, B. Onida, B. Bonelli and E. Garrone, *J. Phys. Chem. B*, 2005, **109**, 16725–16729.
- 56 K. S. W. Sing, *Pure Appl. Chem.*, 1985, **57**, 603–619.
- 57 M. Thommes, K. Kaneko, A. V. Neimark, J. P. Olivier, F. Rodriguez-Reinoso, J. Rouquerol and K. S. W. Sing, *Pure Appl. Chem.*, 2015, **87**, 1051–1069.
- 58 N. La-Salvia, J. J. Lovón-Quintana, A. S. P. Lovón and G. P. Valença, *Mater. Res.*, 2017, **20**, 1461–1469.
- 59 K. Yu, N. Kumar, A. Aho, J. Roine, I. Heinmaa, D. Y. Murzin and A. Ivaska, *J. Catal.*, 2016, **335**, 117–124.
- 60 N. D. Shcherban, S. M. Filonenko, R. Y. Barakov, S. A. Sergiienko, K. Yu, I. Heinmaa, A. Ivaska and D. Y. Murzin, *Appl. Catal., A*, 2017, **543**, 34–42.
- 61 W. Zhao, J. Chu, F. Xie, Q. Duan, L. He and S. Zhang, *J. Chromatogr. A*, 2017, **1485**, 44–51.
- 62 D.-X. Chen, Y.-L. Sun, Y. Zhang, J.-Y. Cui, F.-Z. Shen and Y.-W. Yang, *RSC Adv.*, 2013, **3**, 5765–5768.
- 63 T. Zhou, H. Yu, M. Liu and Y.-W. Yang, *Chin. J. Chem.*, 2015, **33**, 125–130.
- 64 E. C. S. Santos, A. Watanabe, M. D. Vargas, M. N. Tanaka, F. Garcia and C. M. Ronconi, *New J. Chem.*, 2018, **42**, 671–680.
- 65 N. V. Roik and L. A. Belyakova, *Interface Focus*, 2016, **6**, 20160041.
- 66 L. C. Costello and R. B. Franklin, *J. Hum. Endocrinol.*, 2016, **1**, 005.
- 67 P. Icard, L. Poulain and H. Lincet, *Biochim. Biophys. Acta*, 2012, **1825**, 111–116.
- 68 M. E. Mycielska, A. Patel, N. Rizaner, M. P. Mazurek, H. Keun, A. Patel, V. Ganapathy and M. B. A. Djamgoz, *BioEssays*, 2009, **31**, 10–20.
- 69 A. M. Pajor, *Pflugers Arch.*, 2014, **466**, 119–130.
- 70 S. A. Fraenkl, J. Muser, R. Groell, G. Reinhard, S. Orgul, J. Flammer and D. Goldblum, *J. Ocul. Pharmacol. Ther.*, 2011, **27**, 577–580.
- 71 K. Kaur, R. Gupta, S. A. Saraf and S. K. Saraf, *Compr. Rev. Food Sci. Food Saf.*, 2014, **13**, 358–376.
- 72 R. A. Bozym, R. B. Thompson, A. K. Stoddard and C. A. Fierke, *ACS Chem. Biol.*, 2006, **1**, 103–111.
- 73 *Metals and Genetics*, ed. B. Sarkar, Springer US, Boston, MA, 1999.
- 74 W. Maret, *Metallomics*, 2015, **7**, 202–211.
- 75 A. Hervault and N. T. K. Thanh, *Nanoscale*, 2014, **6**, 11553–11573.
- 76 M. I. Majeed, Q. Lu, W. Yan, Z. Li, I. Hussain, W. Tremel, M. N. Tahir and B. Tan, *J. Mater. Chem. B*, 2013, **1**, 2874–2884.
- 77 E. H. Wanderlind, D. G. Liz, A. P. Gerola, R. F. Affeldt, V. Nascimento, L. C. Bretanha, R. Montecinos, L. Garcia-Rio, H. D. Fiedler and F. Nome, *ACS Catal.*, 2018, **8**, 3343–3347.